

Three-dimensional hierarchical conductive metal-organic frameworks/NiFe layered double hydroxide/carbon nanofibers: An efficient oxygen evolution reaction catalyst for Zn-air batteries

Jiajia Li,^a Yunong Qin,^a Yu Lei,^a Shifeng Li,^a Ling Li,^{*a} Bo Ouyang,^{*b} Erjun Kan^b
and Wenming Zhang^{*a}

^a *National-Local Joint Engineering Laboratory of New Energy Photoelectric Devices, College of Physics Science and Technology, Hebei University, Baoding, Hebei 071002, China.*

^b *MIIT Key Laboratory of Semiconductor Microstructure and Quantum Sensing, Nanjing University of Science and Technology, Nanjing 210094, China.*

Corresponding author:

E-mail: lilinghbu@163.com (L. Li), ouyangboyi@njust.edu.cn (B. Ouyang),
wmzhanghbu@126.com (W. Zhang)

Supplementary Figures and Tables

List of Contents

1. Supplementary Figs:

Fig. S1 Preparation and Characterization of Catalysts. a) electrospun sheet, b) carbonized electrospun sheet, c) the sheet after the first hydrothermal reaction and d) the sheet after the second hydrothermal reaction.

Fig. S2 Electron microscopy measurements. (a-d) SEM images of the pure Co-CAT, Co-CAT/CNFs, pure NiFe-LDH and Co-CAT/NiFe-LDH.

Fig. S3 (a) XPS spectrum of the Co-CAT/NiFe-LDH/CNFs. (b) N₂ adsorption/desorption isotherms of samples. (c) Pore diameter distribution image of Co-CAT/NiFe-LDH/CNFs and NiFe-LDH/CNFs.

Fig. S4 (a) XPS Ni 2p spectra, (b) XPS Fe 2p spectra and (c) XPS Co 2p spectra of Co-CAT/NiFe-LDH/CNFs, NiFe-LDH/CNFs and Co-CAT/CNFs.

Fig. S5 (a) XPS Co 2p spectra, (b) XPS Ni 2p spectra and (c) XPS Fe 2p spectra of Co-CAT, Co-CAT/CNFs, NiFe-LDH and NiFe-LDH/CNFs.

Fig. S6 Multi-current process chronopotentiometric curve of the Co-CAT/NiFe-LDH/CNFs.

Fig. S7 ORR performance of the as-prepared products in 0.1 M KOH solution.

Fig. S8 Top view and side view of the initial structure (I) and the structures after adsorption of OH* (II), O* (III), and OOH* (IV) of NiFe-LDH/CNFs, respectively.

Fig. S9 Simplified diagram showing the OER mechanism on the Co-CAT/NiFe-LDH/CNFs electrocatalyst.

Fig. S10 Round-trip efficiency for the 1st, 50th and 100th cycles.

2. Supplementary Tables:

Table S1 The detailed determination of cobalt, nickel, iron, oxide and carbon calculated by means of ICP-MS and EA methods for the Co-CAT/NiFeLDH/CNFs.

Table S2 Comparisons of the OER activity of non-precious metal based electrocatalysts.

Table S3 Power density of Zn-air battery based on non-precious metal based electrocatalysts in alkaline environment.

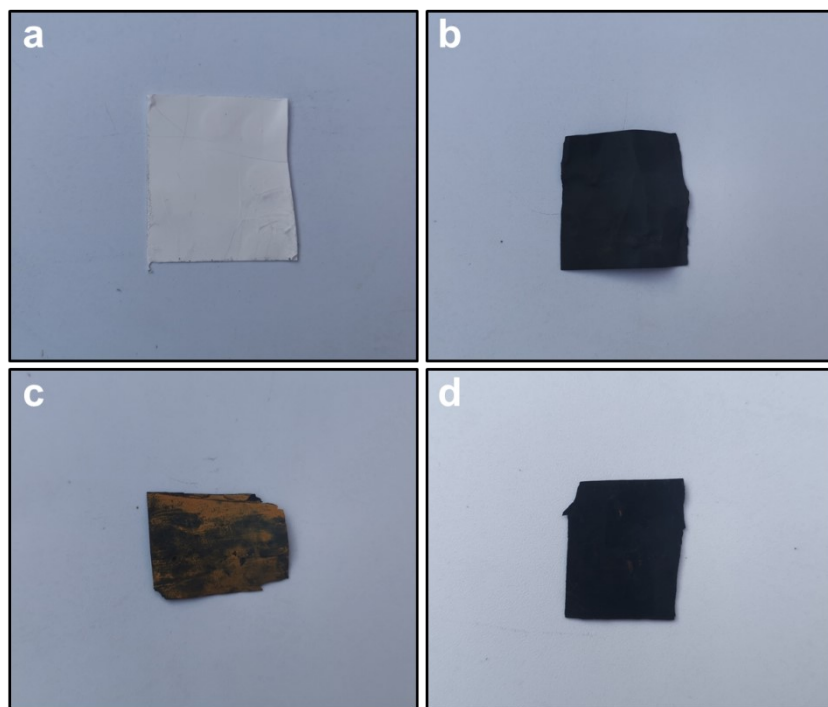


Fig. S1 Preparation and Characterization of Catalysts. a) electrospun sheet, b) carbonized electrospun sheet, c) the sheet after the first hydrothermal reaction and d) the sheet after the second hydrothermal reaction.

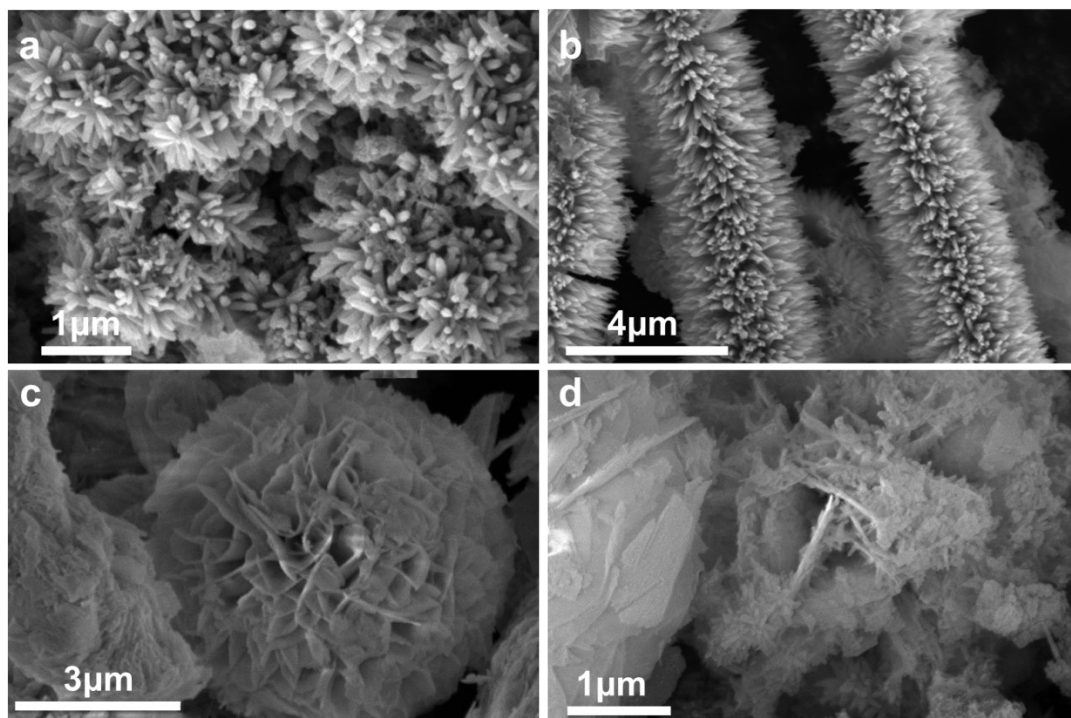


Fig. S2 Electron microscopy measurements. (a-d) SEM images of the pure Co-CAT, Co-CAT/CNFs, pure NiFe-LDH and Co-CAT/NiFe-LDH.

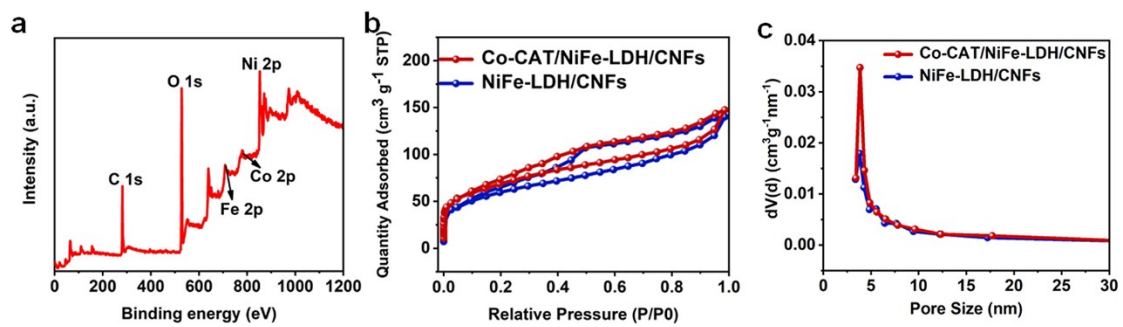


Fig. S3 (a) XPS spectrum of the Co-CAT/NiFe-LDH/CNFs. (b) N₂ adsorption/desorption isotherms of samples. (c) Pore diameter distribution image of Co-CAT/NiFe-LDH/CNFs and NiFe-LDH/CNFs.

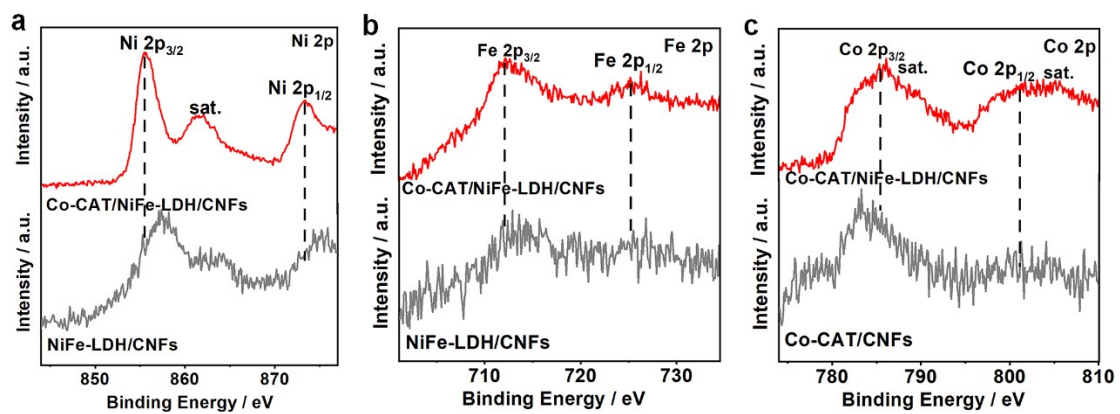


Fig. S4 (a) XPS Ni 2p spectra, (b) XPS Fe 2p spectra and (c) XPS Co 2p spectra of Co-CAT/NiFe-LDH/CNFs, NiFe-LDH/CNFs and Co-CAT/CNFs.

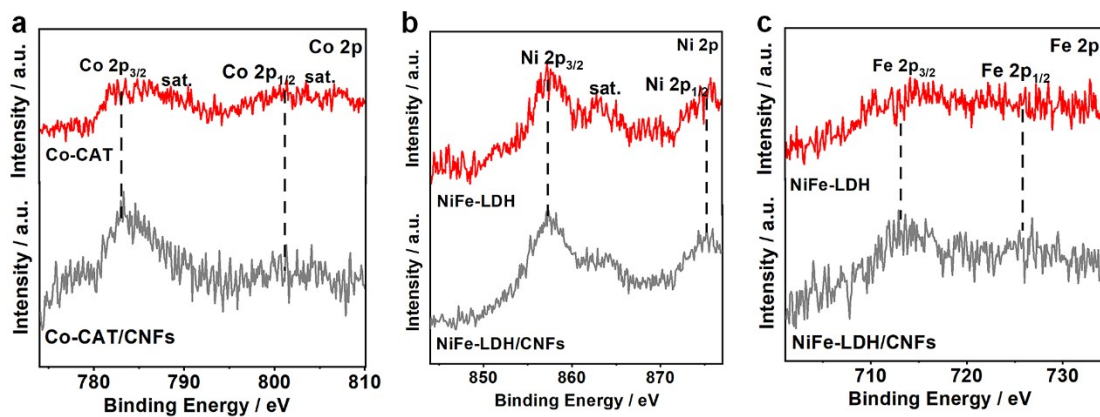


Fig. S5 (a) XPS Co 2p spectra, (b) XPS Ni 2p spectra and (c) XPS Fe 2p spectra of Co-CAT, Co-CAT/CNFs, NiFe-LDH and NiFe-LDH/CNFs.

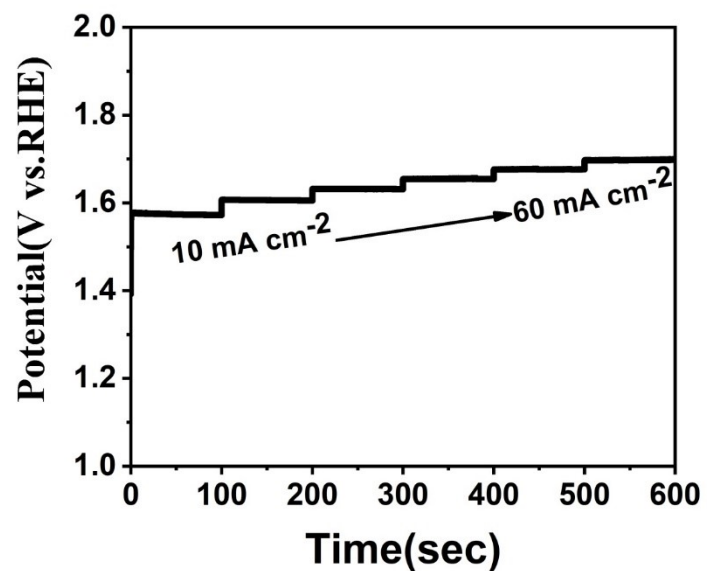


Fig. S6 Multi-current process chronopotentiometric curve of the Co-CAT/NiFe-LDH/CNFs.

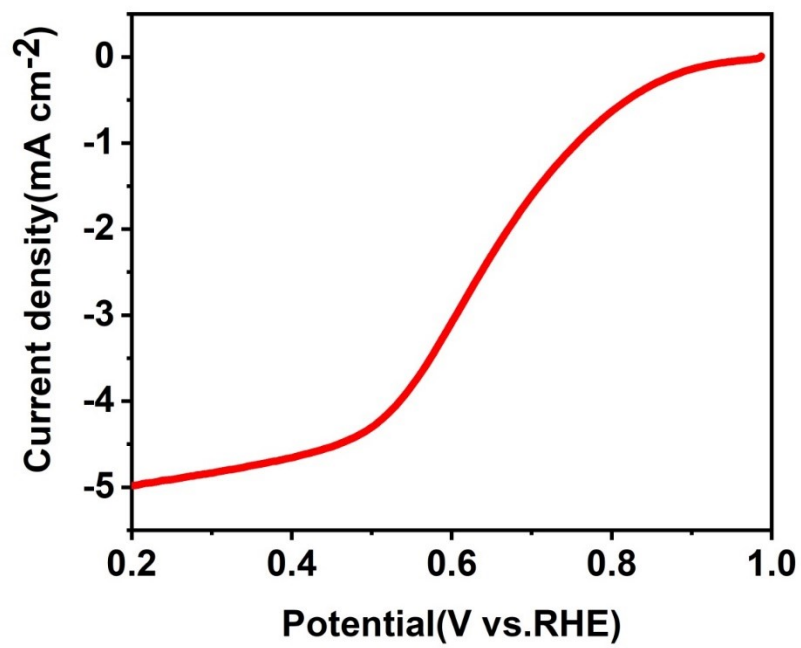


Fig. S7 ORR performance of the as-prepared products in 0.1 M KOH solution.

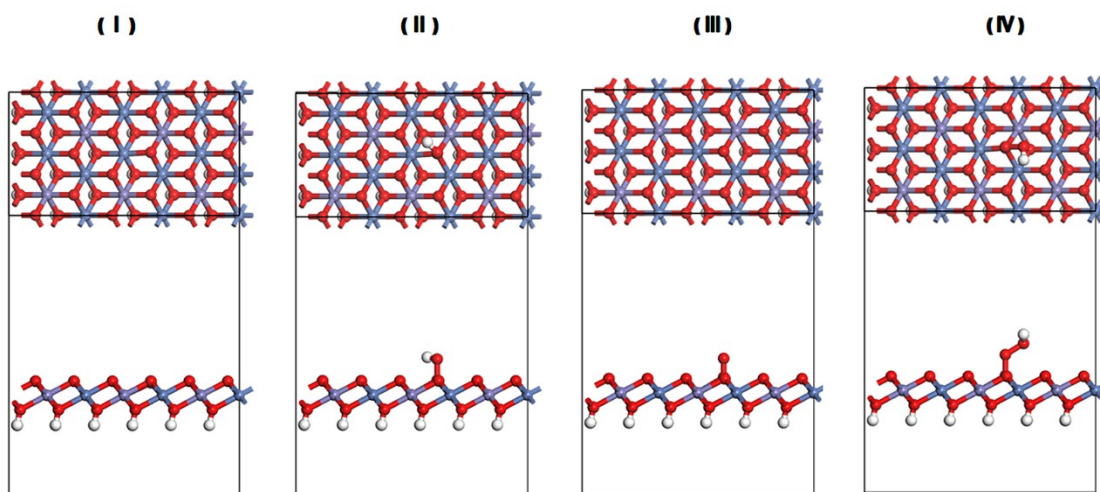


Fig. S8 Top view and side view of the initial structure (I) and the structures after adsorption of OH* (II), O* (III), and OOH* (IV) of NiFe-LDH/CNFs, respectively.

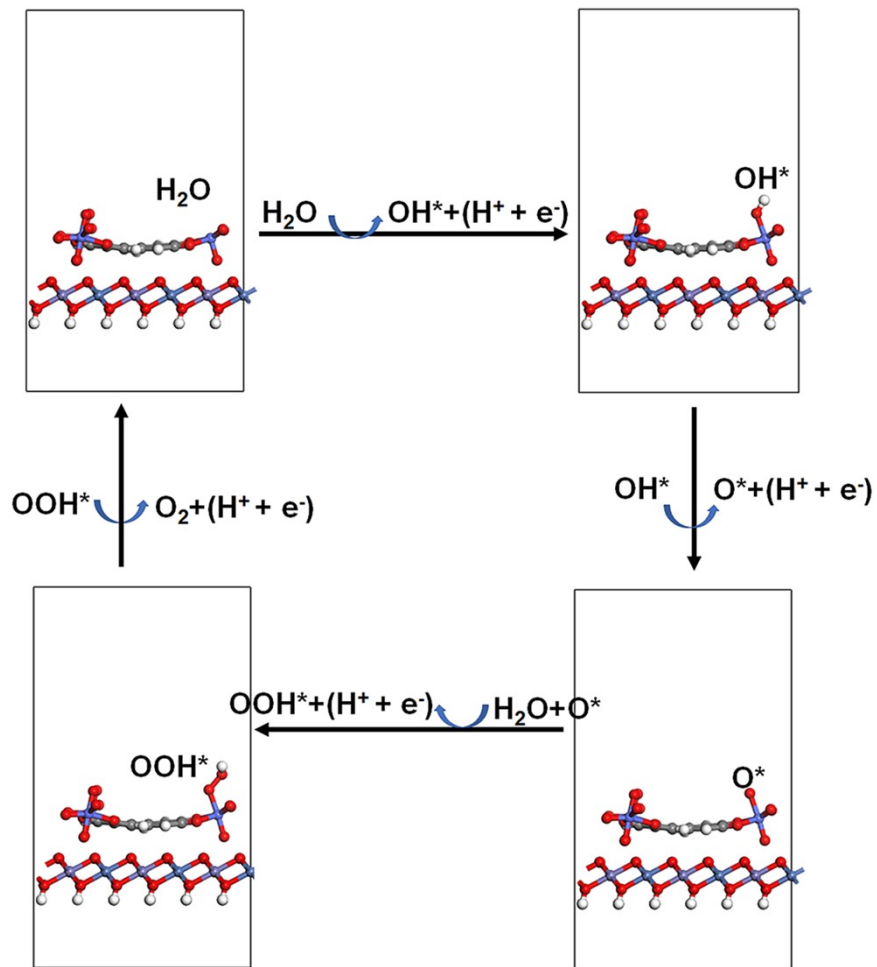


Fig. S9 Simplified diagram showing the OER mechanism on the Co-CAT/NiFe-LDH/CNFs electrocatalyst.

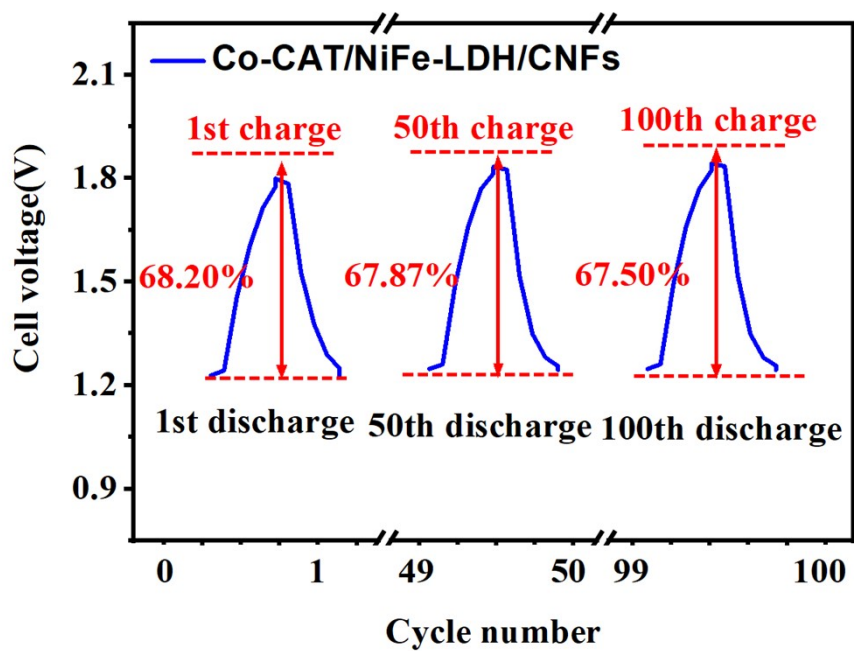


Fig. S10 Round-trip efficiency for the 1st, 50th and 100th cycles.

Table S1 The detailed determination of cobalt, nickel, iron, oxide and carbon calculated by means of ICP-MS and EA methods for the Co-CAT/NiFeLDH/CNFs.

Methods	Sample weight (mg)	Co (g/kg)	Ni (g/kg)	Fe(g/kg)	C (%)	O (%)
ICP-MS	0.0127	15.662	286.647	91.151	-	-
EA	1.956	-	-	-	42.125	-
	1.765	-	-	-	-	14.547

Table S2 Comparisons of the OER activity of non-precious metal based electrocatalysts.

Catalyst	Eleetrolyte	η at J=10 mA cm ⁻² (mV)	Tafel slope (mV dec ⁻¹)	Substrate	scan rate (mV·s ⁻¹)	Ref.
Co-CAT/NiFe-LDH/CNFs	1.0 M KOH	330	85	RDE	10	This work
NiFe-LDH/CNFs	1.0 M KOH	420	121	RDE	10	This work
Co-CAT/CNFs	1.0 M KOH	450	123	RDE	10	This work
RuO ₂	1.0 M KOH	320	91	RDE	10	This work
Pt/C	1.0 M KOH	580	89	RDE	10	This work
MCN-LDH	0.1 M KOH	440	140	RDE	10	S1[1]
Mn-CoN	0.1M KOH	390	57.5	RDE	5	S2[2]
Co-NC@LDH	0.1 M KOH	389	79.65	GC	5	S3[3]
Au-NWs/Ni ₆ MnO ₈	0.1 M KOH	360	62	RDE	5	S4[4]
Ti ₃ C ₂ T _x -CoBDC	0.1M KOH	410	48.2	GC	1	S5[5]
Co-CoOx/N-C	1.0 M KOH	420	71.5	Carbon cloth	5	S6[6]
NiFe-LDH/Co ₃ N-CNF	0.1M KOH	312	60	GC	10	S7[7]
Ni ₃ Fe-Co ₉ S ₈ /rGO	0.1 M KOH	390	109.8	-	5	S8[8]
SNCF-NR	0.1M KOH	390	61	RDE	5	S9[9]
W ₁ Co ₃ S@HCF	1.0 M KOH	437	99	GCE	5	S10[10]
FeCo/FeCoNi@NCNTs-HF	0.1M KOH	378	57	GC	5	S11[11]

Table S3 Power density of Zn-air battery based on non-precious metal based electrocatalysts in alkaline environment.

Catalysts	Electrolyte	Active area (cm ²)/mass loading (mg cm ⁻²)	Power density of ZAB (mW cm ⁻²)	Power density of solid-state ZAB (mW cm ⁻²)	Ref.
Co-CAT/NiFe-LDH/CNFs	6.0 M KOH	1	327.09	112.04	This work
NiFe-LDH/CNFs	6.0 M KOH	1	49.97	65.2	This work
Pt/C	6.0 M KOH	1	101.92	71.41	This work
MCN-LDH	6.0 M KOH and 0.2 M ZnCl ₂	3 mg cm ⁻²	-	-	S1
Mn-CoN	6.0 M KOH+0.2 M Zn(Ac) ₂	1	53	-	S2
Co-NC@LDH	6.0 M KOH + 0.2 M Zn(Ac) ₂	3 mg cm ⁻²	107.8	-	S3
Au-NWs/Ni ₆ MnO ₈	6.0 M KOH + 0.20 M ZnCl ₂	-	121	-	S4
Ti ₃ C ₂ Tx-CoBDC	6 M KOH + 0.2 M Zn(Ac) ₂ ·2 H ₂ O	~2.5 mg cm ⁻²	-	-	S5
Co-CoOx/N-C	PVA gel	-	-	20.7	S6
NiFe-LDH/Co,N-CNF	6 M KOH and 0.2 M	1 mg cm ⁻²	-	-	S7

Ni ₃ Fe-Co ₉ S ₈ /rGO	zinc acetate 0.2 M ZnCl ₂ + 6 M KOH	10 mg cm ⁻²	125	-	S8
FeCo/FeCoNi@NCNTs -HF	6 M KOH + 0.2 M Zn(ac) ₂	2.0 mg cm ⁻²	156.22	-	S11

References

- [1] Y. Qian, T. An, E. Sarnello, Z. Liu, T. Li and D. Zhao, Janus electrocatalysts containing MOF-derived carbon networks and NiFe-LDH nanoplates for rechargeable zinc-air batteries, *ACS Appl. Energy Mater.*, 2019, **2**, 1784-1792.
- [2] Y. Zhang, B. Ouyang, G. Long, H. Tan, Z. Wang, Z. Zhang, W. Gao, R. Rawat and H. Fan, Enhancing bifunctionality of CoN nanowires by Mn doping for long-lasting Zn-air batteries, *Sci. China. Chem.*, 2020, **63**, 890-896.
- [3] D. Chen, X. Chen, Z. Cui, G. Li, B. Han, Q. Zhang, J. Sui, H. Dong, J. Yu, L. Yu and L. Dong, Dual-active-site hierarchical architecture containing NiFe-LDH and ZIF-derived carbon-based framework composite as efficient bifunctional oxygen electrocatalysts for durable rechargeable Zn-air batteries, *Chem. Eng. J.*, 2020, **399**, 125718.
- [4] G. Fu, X. Jiang, Y. Chen, L. Xu, D. Sun, J.-M. Lee and Y. Tang, Robust bifunctional oxygen electrocatalyst with a “rigid and flexible” structure for air-cathodes, *NPG Asia Mater.*, 2018, **10**, 618-629.
- [5] H. Cheng, M. Li, C. Su, N. Li and Z. Liu, Cu-Co bimetallic oxide quantum dot decorated nitrogen-doped carbon nanotubes: A high-efficiency bifunctional oxygen electrode for Zn-air batteries, *Adv. Funct. Mater.*, 2017, **27**, 1701833.
- [6] S. Li, W. Xie, Y. Song and M. Shao, Layered double hydroxide@polydopamine core-shell nanosheet arrays-derived bifunctional electrocatalyst for efficient, flexible,

- all-solid-state zinc-air battery, *ACS Sustain. Chem. Eng.*, 2019, **8**, 452-459.
- [7] Q. Wang, L. Shang, R. Shi, X. Zhang, Y. Zhao, G. Waterhouse, L. Wu, C. Tung and T. Zhang, NiFe layered double hydroxide nanoparticles on Co,N-codoped carbon nanoframes as efficient bifunctional catalysts for rechargeable zinc-air batteries, *Adv. Energy Mater.*, 2017, **7**, 1700467.
- [8] X. Hu, T. Huang, Y. Tang, G. Fu and J. Lee, Three-dimensional graphene-supported Ni₃Fe/Co₉S₈ composites: rational design and active for oxygen reversible electrocatalysis, *ACS Appl. Mater. Interfaces*, 2019, **11**, 4028-4036.
- [9] Y. Zhu, W. Zhou, Y. Zhong, Y. Bu, X. Chen, Q. Zhong, M. Liu and Z. Shao, A perovskite nanorod as bifunctional electrocatalyst for overall water splitting, *Adv. Energy Mater.*, 2017, **7**, 1602122.
- [10] T. Zhou, W. Xu, N. Zhang, Z. Du, C. Zhong, W. Yan, H. Ju, W. Chu, H. Jiang and C. Wu, Ultrathin cobalt oxide layers as electrocatalysts for high-performance flexible Zn-Air batteries, *Adv. Mater.*, 2019, **31**, 1807468.
- [11] Z. Wang, J. Ang, B. Zhang, Y. Zhang, X. Ma, T. Yan, J. Liu, B. Che, Y. Huang and X. Lu, FeCo/FeCoNi/N-doped carbon nanotubes grafted polyhedron-derived hybrid fibers as bifunctional oxygen electrocatalysts for durable rechargeable zinc-air battery, *Appl. Catal. B*, 2019, **254**, 26-36.